The American Journal of Human Genetics, Volume *108*

Supplemental Data

Topologically associating domain boundaries that are stable across diverse cell types are evolutionarily constrained and enriched for heritability

Evonne McArthur and John A. Capra

SUPPLEMENTAL TEXT

TAD maps and length

TAD maps for 37 different cell types were obtained from the 3D genome browser (Table S1). All cell types were available in hg19 format, except the liver data, which we downloaded in hg38 and used the UCSC liftOver tool to convert to hg19 [1,2].The median TAD length across all cell types is 1.15 Mb (IQR: 0.71 - 1.82 Mb) and the median number of TADs per cell type is 1844 (IQR: 1625 - 2277). We observed an inverse relationship between TAD length and number of TADs in a cell type: cells with longer TADs have fewer TADs (Fig. S17). Primary tissues have longer TADs, whereas naïve cell types like stem cells and de-differentiated leukemia cell-lines have shorter TADs (Fig. S17). This is consistent with previous examination of neuronal development which found that, during differentiation, TAD number decreases with a corresponding increase in size [3].

Similarity between TAD maps

Our finding of TAD map similarity among functionally similar cell types contrasts with previous work by Sauerwald *et al.* (2018) that found that most similar TAD map pairs have no biological connection; however, they investigate a different set of cells (predominantly cancer cell lines) [4]. Comparisons with highly mutated cancer cell lines that may not reflect natural boundary patterns. Both our results and the Sauerwald *et al*. 2018 comparisons could be influenced by batch effects because the Hi-C data considered were generated by different groups. However, an important follow-up by Sauerwald *et al.* (2020) finds that lab specific differences have little impact on TAD map similarity comparisons and that cell type is the greater driver of biological variation in TAD structures [5].

Our similarity quantifications agree with some previous estimates. We find that the median pairwise Jaccard similarity for all 37 x 37 cell type comparisons is 0.18 (IQR: 0.15 - 0.23), 0.32 (IQR: 0.26 - 0.37), 0.41 (IQR: 0.35 - 0.47) at 40 kb, 100 kb, and 200 kb resolution, respectively. Our pairwise Jaccard similarity between 200 kb boundaries (0.41) aligns with previous analyses that examined cell type TAD map similarity among larger windows have reported similarity coefficients between 0.4 - 0.5 [4,5]. At a finer resolution, Rao et al. (2014) reported Jaccard indices from 0.21 - 0.30 for comparisons of GM12878 to each of IMR90, HMEC, HUVEC, K562, KBM7 and NHEK [4,6]. The Jaccard similarity for our comparisons of these cell types is 0.24 - 0.37 (40 kb resolution).

Overall, this variability in TAD similarity across different cell types highlights the sensitivity of stability comparisons to the definition of TAD boundaries used. For example, the median pairwise Jaccard similarity between 40 kb boundaries across 21 tissues defined by Schmitt et al. (2016) is 0.106 (IQR: 0.086 - 0.123). However, they collapsed boundaries to 200 kb “boundary regions” to conclude that TAD boundaries are highly stable (stating that over 35% of TAD boundaries are present in 21 of 21 tissues) [7]. These previous studies often investigated more homogenous groups of cell types which could lead to higher estimates of stability. Ultimately, we stress than when interpreting claims of similarity between TAD maps of different cell types, the method of defining TADs (versus loop domains or boundary “regions”), the genomic resolution, and the breadth of cell types considered should be considered for context.

SUPPLEMENTAL FIGURES

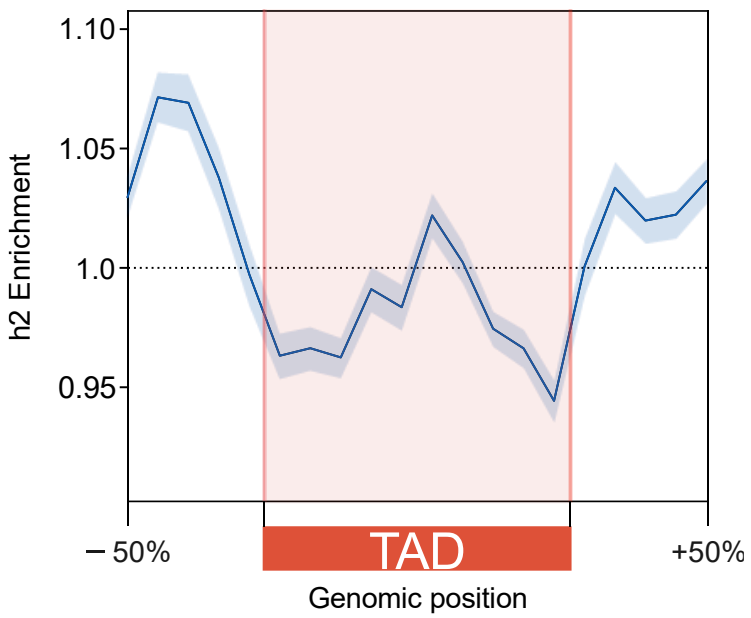

Figure S1. Meta-analysis of heritability patterns across cell types yields similar results to averaging. For TADs across 37 cell types, heritability is enriched near regions flanking TADs when meta-analyzed across 41 common complex phenotypes. When combining data across traits, the heritability enrichment results are consistent using random-effects meta-analysis model (here) versus averaging (r^2 = 0.85, P = 7x10^{-9}, Fig. 2A). The error band signifies a 99% confidence interval.

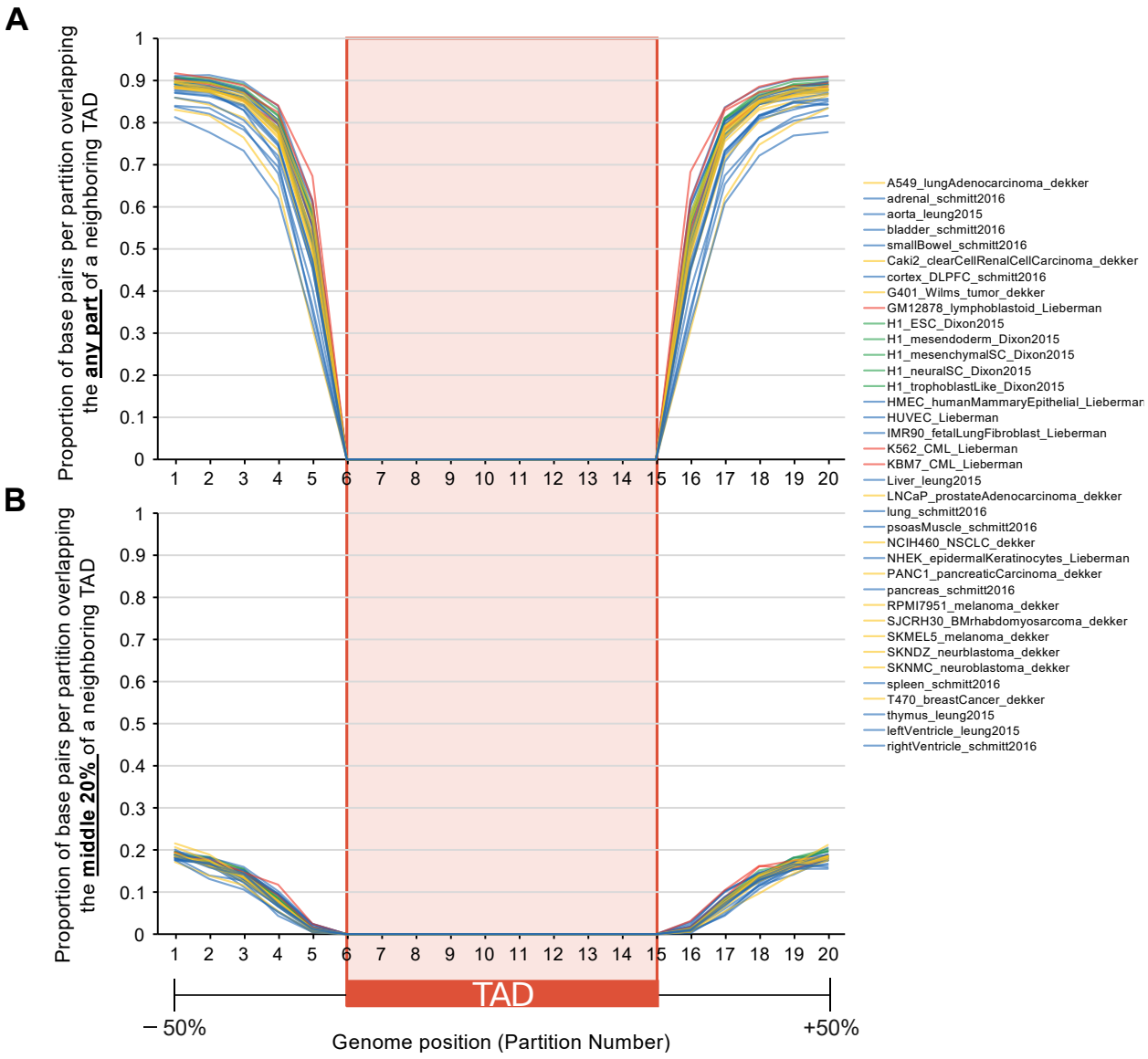

Figure S2. Overlap between region flanking TADs and neighboring TADs. In Fig. 2 and 4A-C we analyzed TADs plus 50% of their total length on each side and subdivided this region into 20 equal-sized partitions. Bins 1-5 and 16-20 "bookend" the TAD, while the center bins 6-15 are inside the TAD. Because TADs are often adjacent, we quantify how often the ±50% region flanking the TAD (bins 1-5,16-20) overlaps a neighboring TAD. Per partition across the TAD landscape (x-axis) we calculate the proportion of bases that overlap **(A)** any part of a neighboring TAD and **(B)** the middle 20% of a neighboring TAD. A higher proportion of the partitions further from the edge of the TAD overlap a neighboring TAD, as expected. At the bin farthest from the TAD (bins 1 and 20), 80-90% extend into a neighboring TAD. However, less than 20% extend into the center of a neighboring TAD.

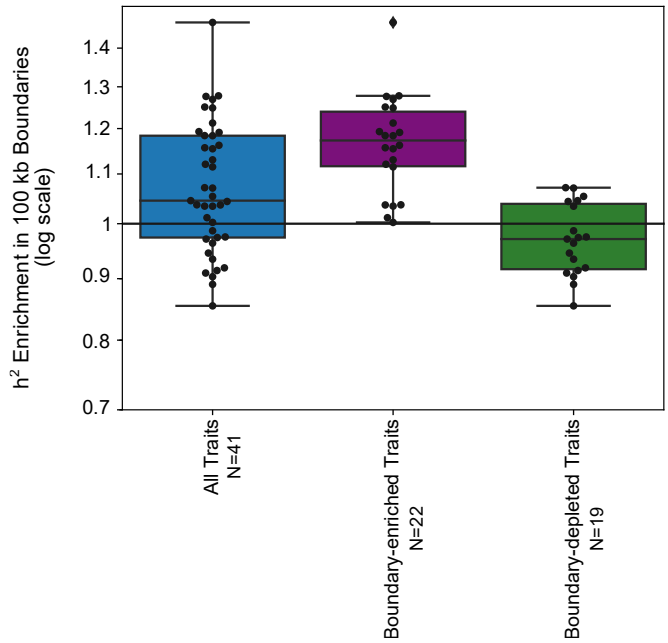

Figure S3. TAD boundaries are enriched for heritability. When defining TAD boundaries as the 100 kb region flanking TADs, boundaries are generally enriched for heritability across 41 common complex traits (blue box, 1.07x, *P* = 0.001). These are the same data shown in Fig. 3C; however, the boundaries are not stratified by their stability across cell types. When we split the traits into the clusters defined in Fig. 4, Boundary-enriched traits are further enriched for trait heritability (purple box, 1.16x, $P = 1x10^{-7}$) while Boundary-depleted traits show no significant enrichment (green box, 0.97x, *P* = 0.06). These are the same data shown in Fig. 4D and 4F, respectively, without stratification by stability across cell types. These findings are consistent with the heritability patterns across the TAD landscapes shown in Fig. 2A, 4B-C, but with fixed-window 100 kb boundary definitions.

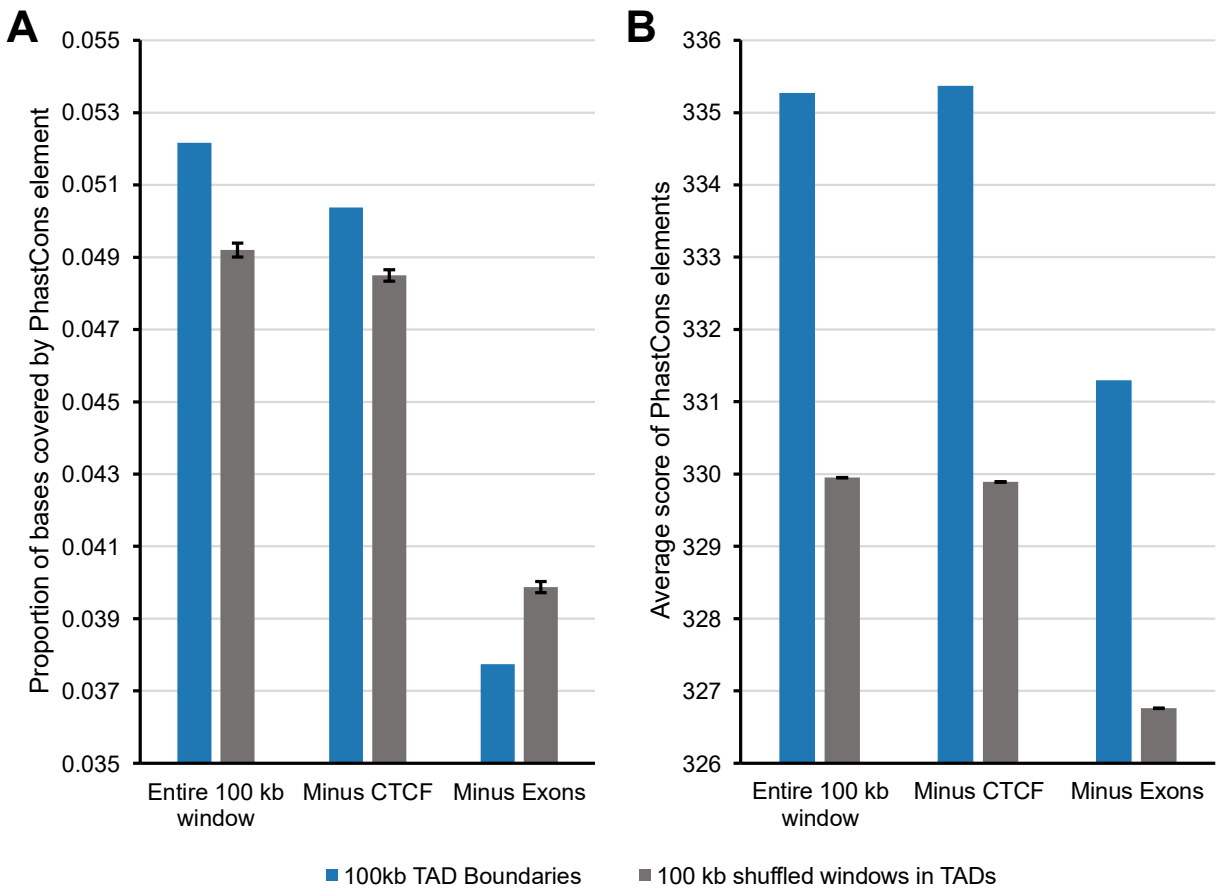

Figure S4. TAD boundaries are more conserved than windows inside TADs. We quantified evolutionary sequence conservation in terms of **(A)** the proportion of base pairs in a region overlapping a conserved element identified by PhastCons and **(B)** by the element-wise average PhastCons conservation score across the region. Using these two measures we compared base pair level conservation in 100 kb TAD boundaries (blue) and matched 100 kb windows shuffled inside TADs (n = 111, gray). When considering the entire 100 kb window, TAD boundaries have more overlap with PhastCons elements and a higher average PhastCons element score than windows in TADs (left bars). When considering the 100 kb windows with CTCF ChIP-seq peaks removed, TAD boundaries still have more overlap and higher score than windows in TADs (middle bars). When considering the 100 kb windows with all exons removed, TAD boundaries have less overlap with PhastCons elements, but the remaining PhastCons elements still have a higher conservation score (right bars).

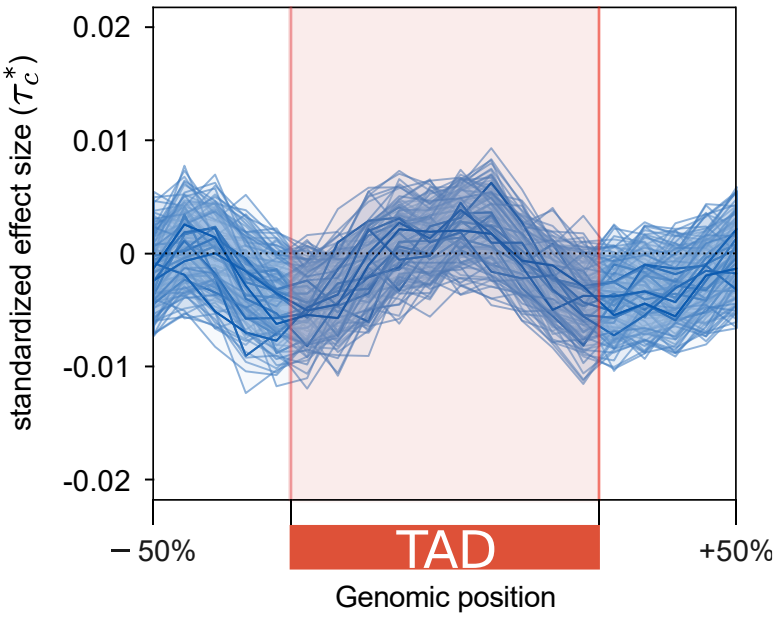

Figure S5. Trait heritability conditioned on 86 annotations. In contrast to heritability enrichment, the standardized effect size (τ^*_c) quantifies effects that are unique to the focal annotation compared to a set of other 86 annotations (*e.g.* regulatory annotations, evolutionary conservation, coding regions, LD, minor allele frequency). When meta-analyzed across all traits, the standardized effect sizes for partitions across the 3D genome are non-significant compared to the unconditioned enrichment analyses (Fig. 2). This indicates that enrichment for these known annotations (e.g., CTCF binding sites and genes) across partitions explains much of the observed heritability enrichment for regions flanking TADs. Each line represents the standardized effect size meta-analyzed across all traits for that cell type (n = 37). The error bands signify 99% confidence intervals.

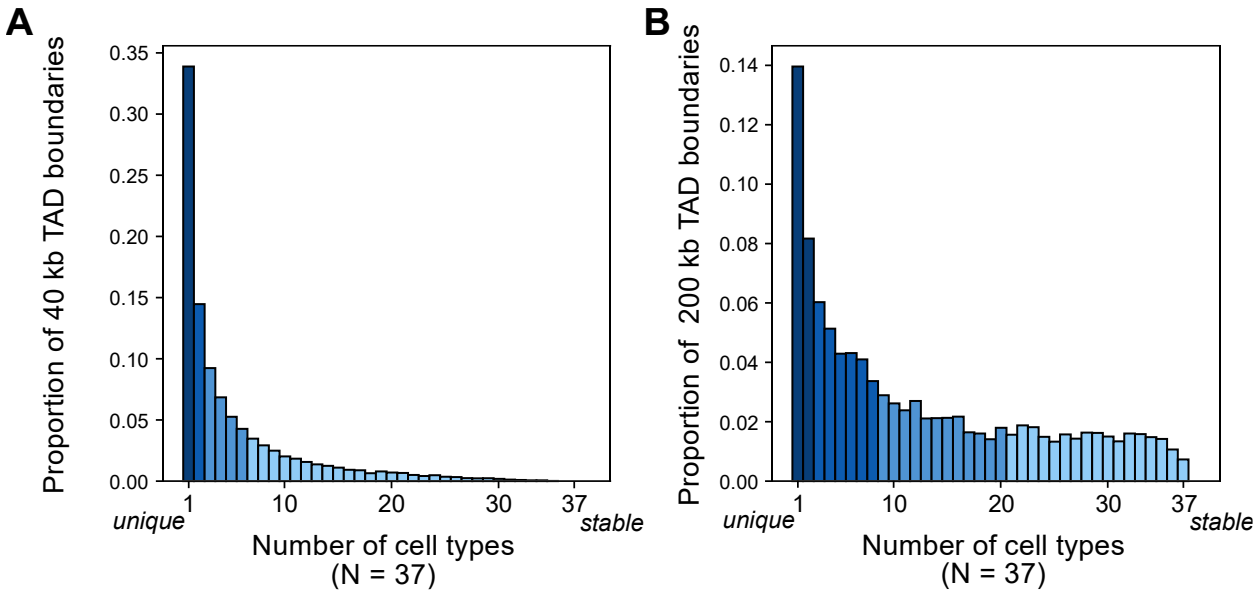

Figure S6. Histograms of boundary stability based on alternate definitions of TAD boundaries. Histograms of TAD boundaries by the number of cell types they are observed in (their "stability") colored by quartiles. In addition to the 100 kb bookend boundary definitions (Fig. 3B), our supplemental analysis investigates **(A)** 40 kb centered boundaries and **(B)** 200 kb bookend boundaries (Methods). Using the 40 kb definition, 33.9% of boundaries are unique to a single context and 2.0% of boundaries are observed in 25+ of 37 cell types. Using the 200 kb definition, 14.0% of boundaries are unique to a single context and 18.3% of boundaries are observed in 25+ of 37 cell types.

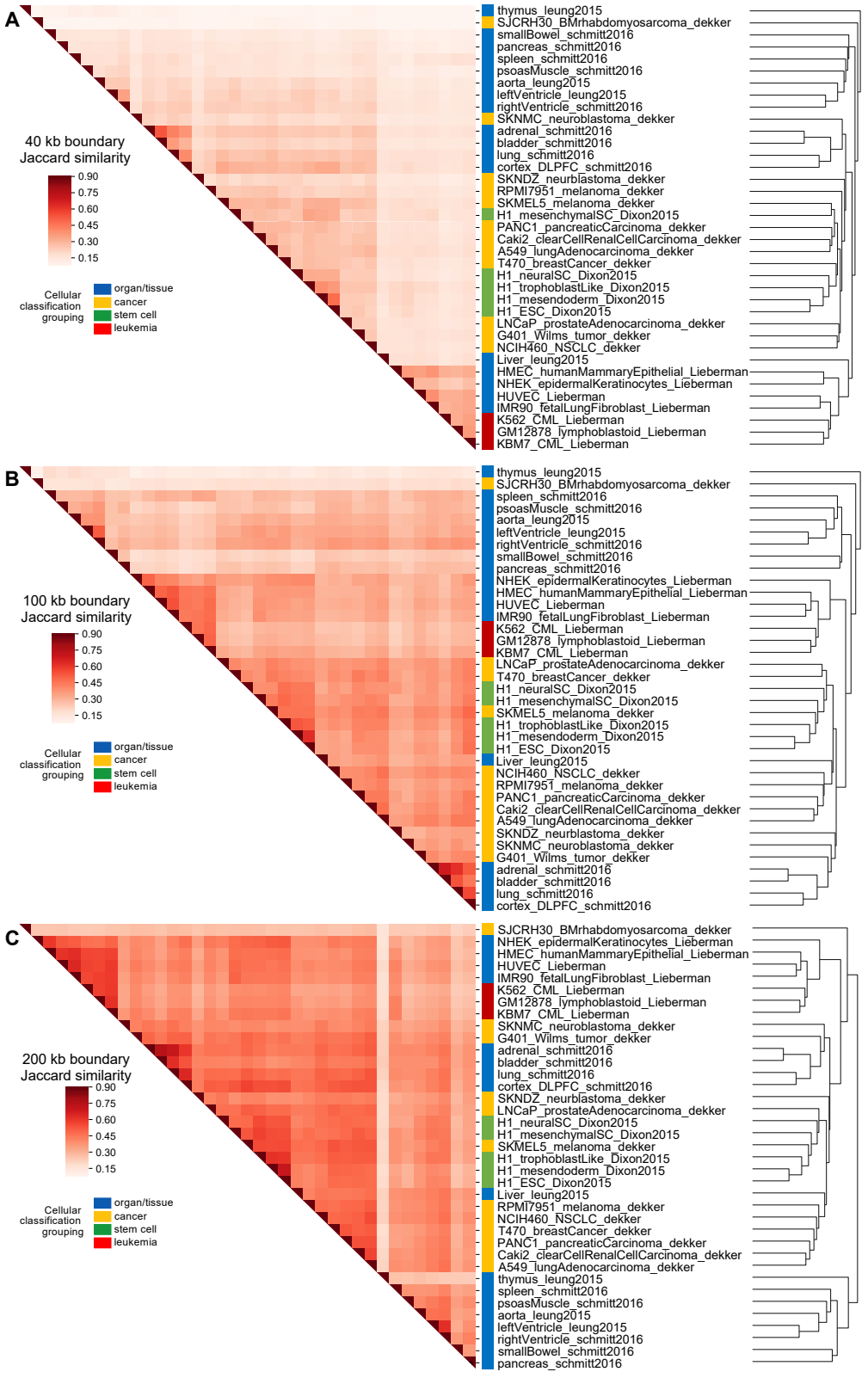

Figure S7. Biologically similar cell types cluster by TAD map similarity. Clustering for 37 cell types using the pairwise Jaccard similarity metric with colors labelling cellular groups for **(A)** 40 kb boundaries, **(B)** 100 kb boundaries, and **(C)** 200 kb boundaries.

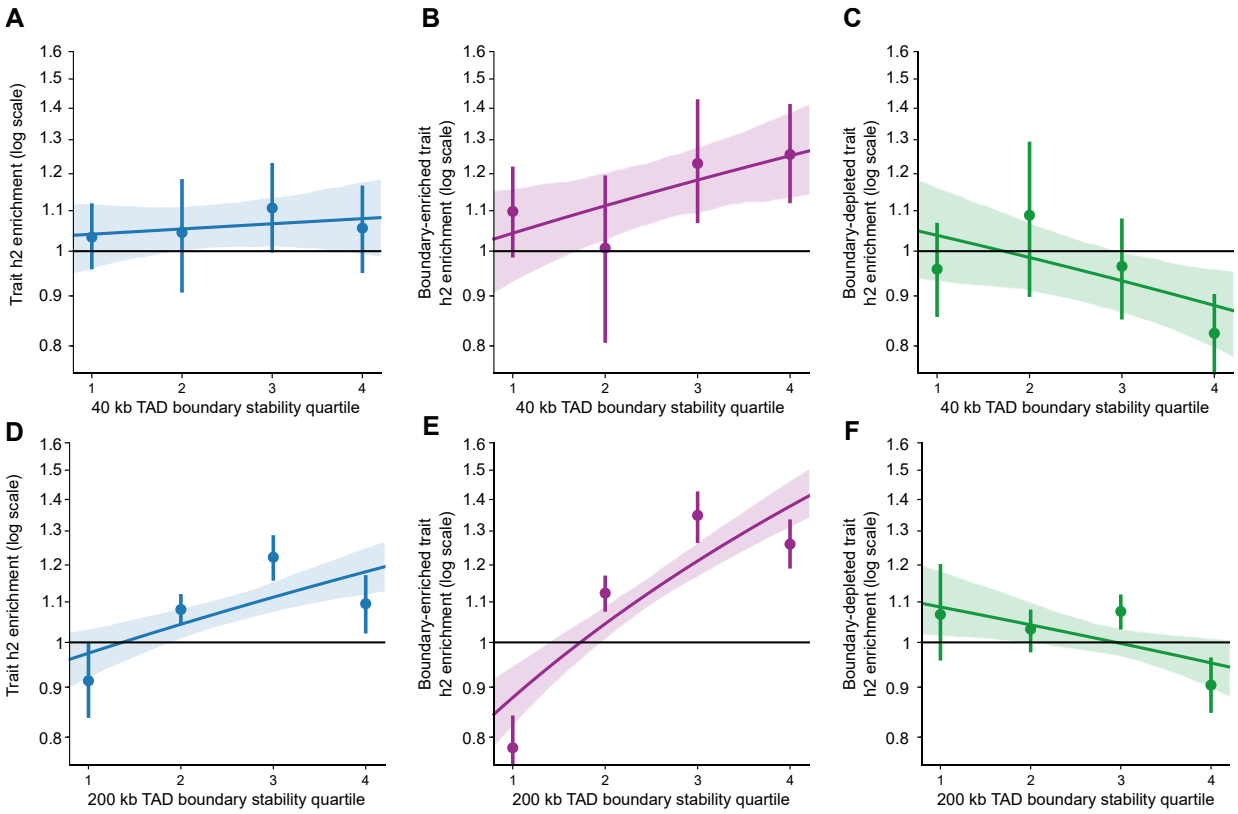

Figure S8. Relationship between heritability enrichment and boundary stability is robust to different boundary definitions. Over all traits, there is a positive relationship between boundary stability and heritability enrichment using 40 kb boundaries (**A**, $P = 0.61$), 100 kb boundaries (Fig. 3C, $P = 0.006$), and 200 kb boundaries (**D**, $P = 2 \times 10^{-5}$). For traits in the boundary-enriched cluster (Fig. 4B), there is a stronger positive relationship between boundary stability and heritability in 40 kb boundaries (**B**, $P = 0.06$), 100 kb boundaries (Fig. 4D, $P = 2 \times 10^{-6}$), and 200 kb boundaries (**E**, $P = 3 \times 10^{-14}$). For traits in the boundary-depleted cluster (Fig. 4C), there is a weak negative relationship between boundary stability and heritability using 40 kb boundaries (**C**, $P = 0.09$), 100 kb boundaries (Fig. 4F, $P = 0.09$), and 200 kb boundaries (**F**, $P = 0.01$). Error bars/bands signify 95% confidence intervals.

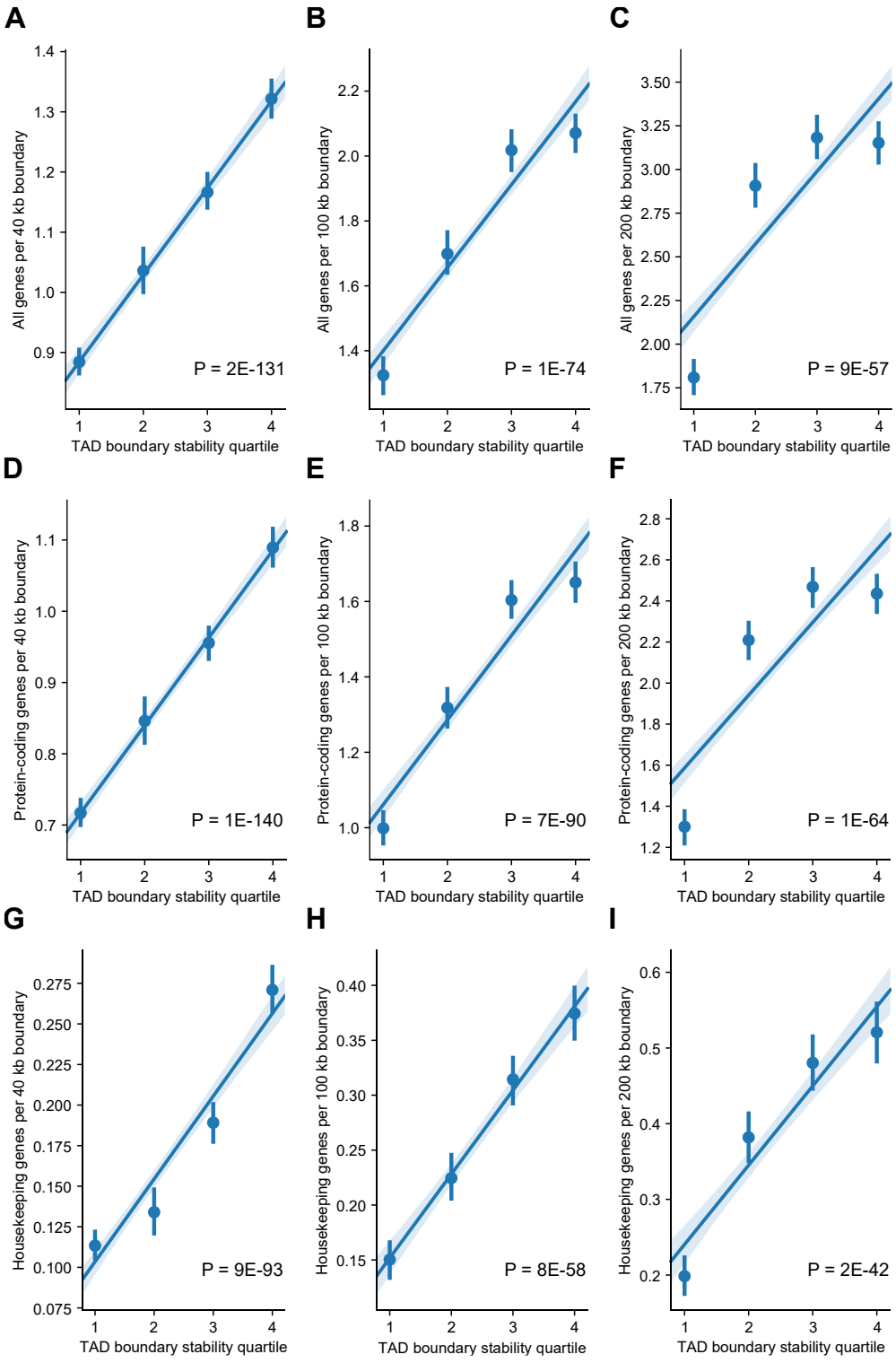

Figure S9. The enrichment of stable TAD boundaries for genes is robust to gene set and boundary definitions. The relationship between increased TAD boundary stability and gene overlap using 40 kb boundaries **(A,D,G)**, 100 kb boundaries **(B,E,H)**, and 200 kb boundaries **(C,F,I)**. We also demonstrate this trend using three types of genes: all RefSeq genes **(A-C)**, protein-coding genes **(D-F)**, and housekeeping genes **(G-I)**. Panel H is shown in the main text (Fig. 3F). TAD boundary stability quartiles are defined by the empirical distributions shown in Fig. S6A (40 kb), Fig. 3B (100 kb), and Fig. S6B (200 kb). Boundaries in the first quartile are unique to a single cell type, while boundaries in higher quartiles are stable across multiple cell types. Error bars/bands signify 95% confidence intervals.

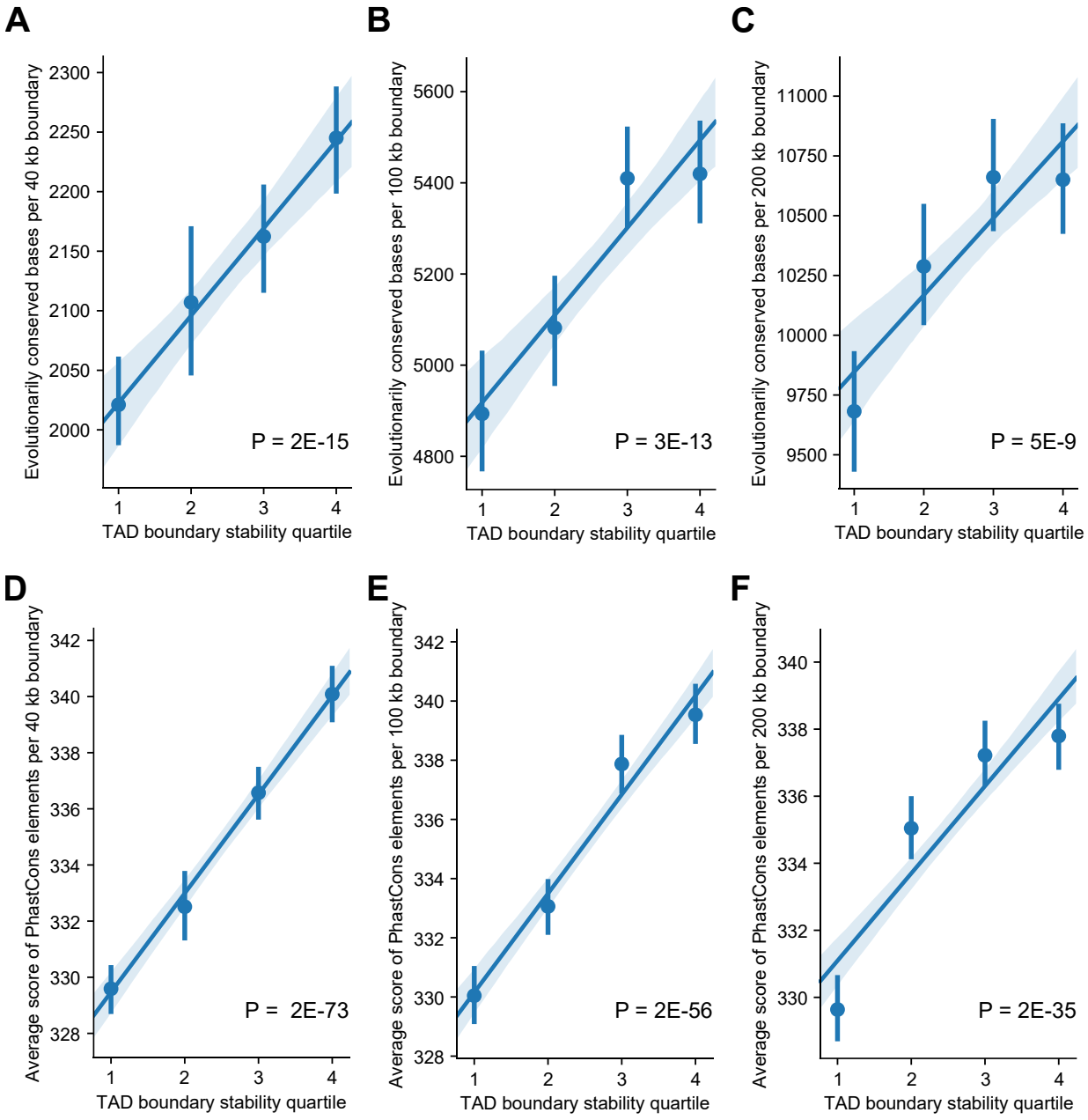

Figure S10. The enrichment of stable TAD boundaries for sequence-level conservation is robust to boundary definitions. The relationship between increased TAD boundary stability and sequence-level conservation quantified (via PhastCons element overlap) considering 40 kb boundaries **(A & D)**, 100 kb boundaries **(B & E)**, and 200 kb boundaries **(C & F)**. We also demonstrate this trend holds with two different measures of evolutionary conservation: number of bases overlapping PhastCons elements **(A-C)** and average PhastCons element score per boundary **(D-F)**. Panel B is shown in the main text (Fig. 3D). TAD boundary stability quartiles are defined by the empirical distributions shown in Fig. S6A (40 kb), Fig. 3B (100 kb), and Fig. S6B (200 kb). Boundaries in the first quartile are unique to a single cell type, while boundaries in higher quartiles are stable across multiple cell types. Error bars/bands signify 95% confidence intervals.

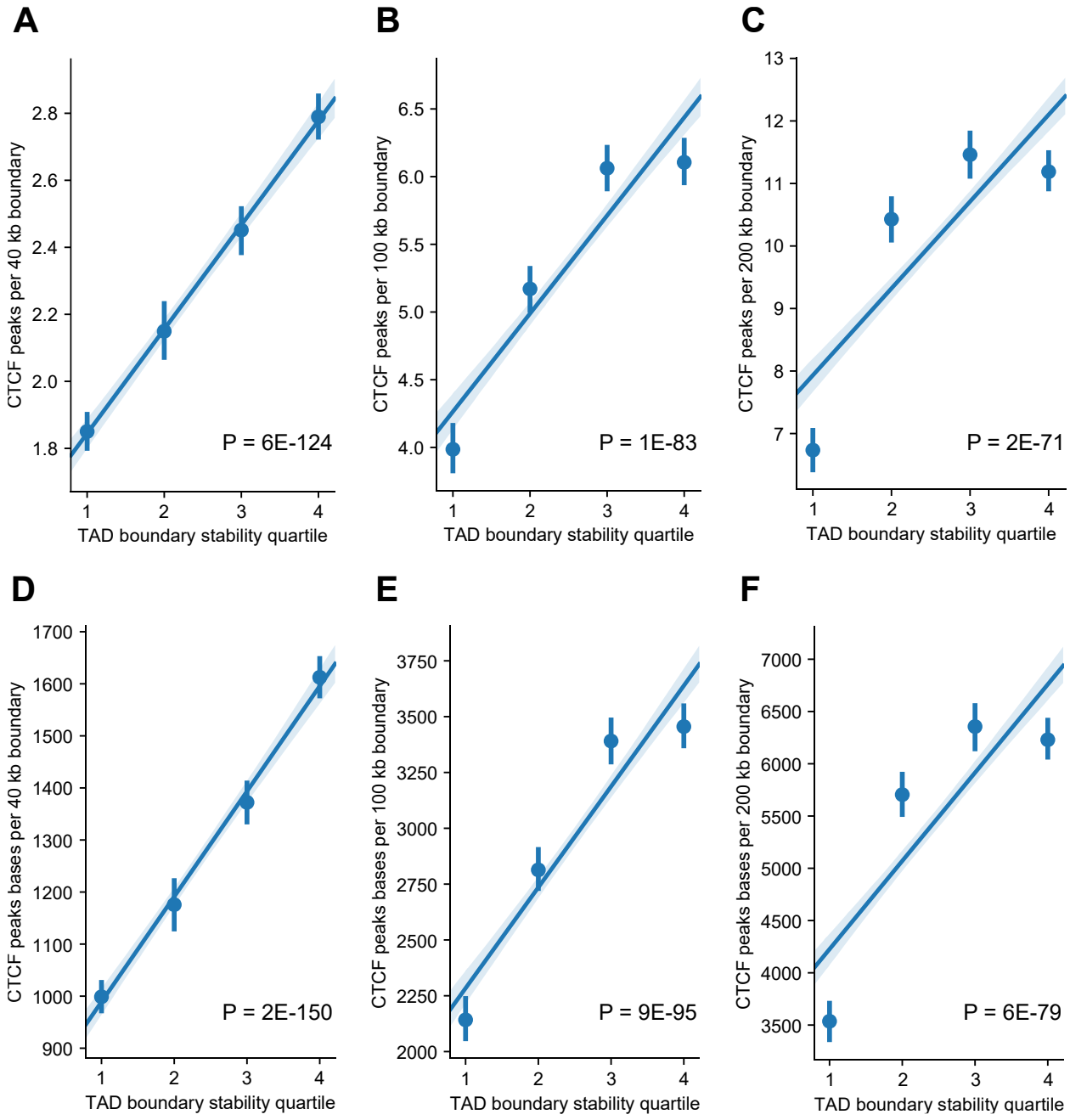

Figure S11. The enrichment of stable TAD boundaries for CTCF binding is robust to boundary definitions. The relationship between increased TAD boundary stability and CTCF binding considering 40 kb boundaries **(A & D)**, 100 kb boundaries **(B & E)**, and 200 kb boundaries **(C & F)**. We also demonstrate this trend holds with two different quantifications of CTCF overlap: count of CTCF ChIP-seq peaks per boundary **(A-C)** and number of CTCF ChIP-seq peak bases overlapping each boundary **(D-F)**. Panel B is shown in the main text (Fig. 3E). TAD boundary stability quartiles are defined by the empirical distributions shown in Fig. S6A (40 kb), Fig. 3B (100 kb), and Fig. S6B (200 kb). Boundaries in the first quartile are unique to a single cell type, while boundaries in higher quartiles are stable across multiple cell types. Error bars/bands signify 95% confidence intervals.

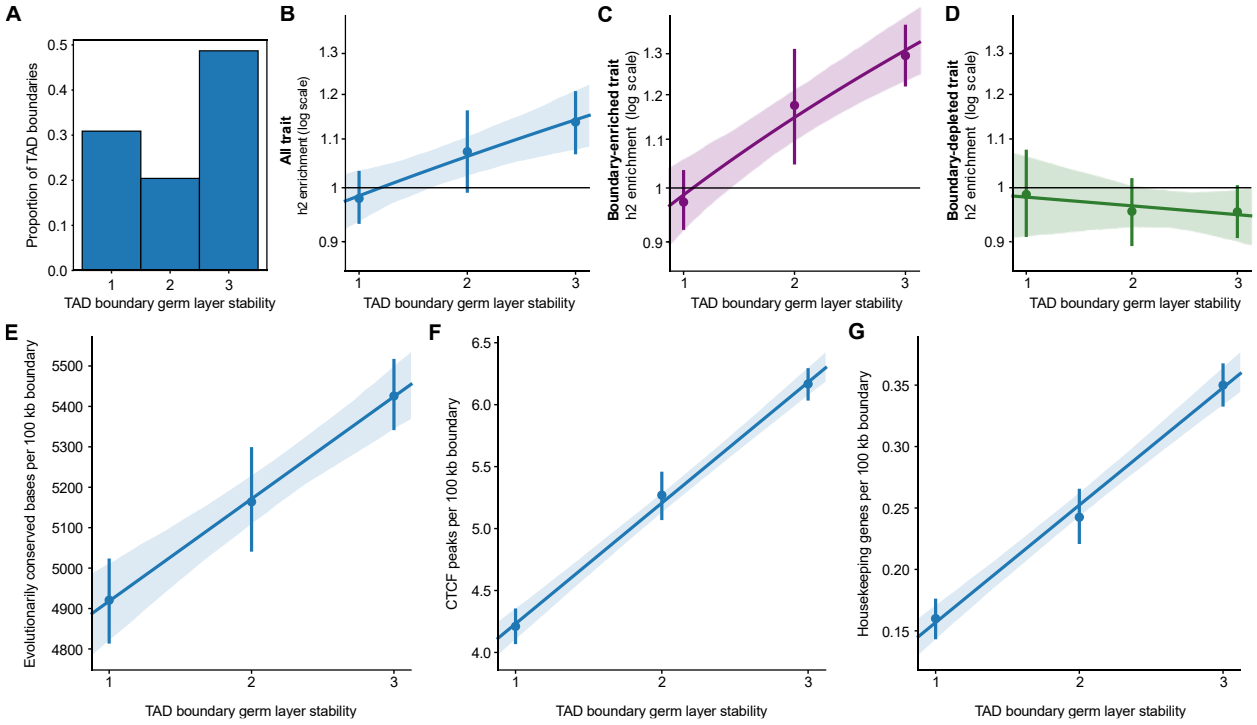

Figure S12. Heritability enrichment and conservation at TAD boundaries stable across cell types replicates using a germ-layer-informed measure of stability. Of the 37 cell types considered, some are more closely related than others, therefore we grouped 34 of them by germ layer (endoderm [N=12], mesoderm [N=13], ectoderm [N=9]; Table S1). We then quantified stability based on whether the boundary was found in one, two, or all three germ layers. **(A)** The proportion of 100 kb boundaries that fall into each stability measurement. For example, if a boundary was found in muscle, spleen, and mesenchymal stem cells, but no other tissues, it is a "mesoderm-only" boundary and in the "1" category for germ layer stability. If a boundary was found in muscle, cortex, and lung, it is a boundary found across all three germ layers and in the "3" category for germ layer stability. These examples were assigned the same level of stability in the raw cell type count measure because they are both present in 3/37 cell types (Fig. 3, 4D, and 4F). Increased stability using this germ layer informed measure is correlated with increased: **(B)** complex trait heritability enrichment (P = 0.002), **(E)** conserved bases (overlap with PhastCons elements, $P = 2\text{x}10^{-14}$), **(F)** CTCF binding (overlap with ChIP-seq peaks, $P = 3\text{x}10^{-97}$), and **(G)** housekeeping genes ($P = 3\text{x}10^{-58}$). When we split the traits into the clusters defined in Fig. 4, **(C)** the positive correlation between boundary stability and trait heritability is even stronger for the subset of traits in the boundary-enriched cluster ($P = 2\text{x}10^{-5}$), while **(D)** the boundary-depleted traits show no significant trend between boundary stability and trait heritability (P = 0.49). Respectively, these replicate the results in Figs. 3C-F, 4D, and 4F with the germ-layer stability measurement. All error bars/bands signify 95% confidence intervals.

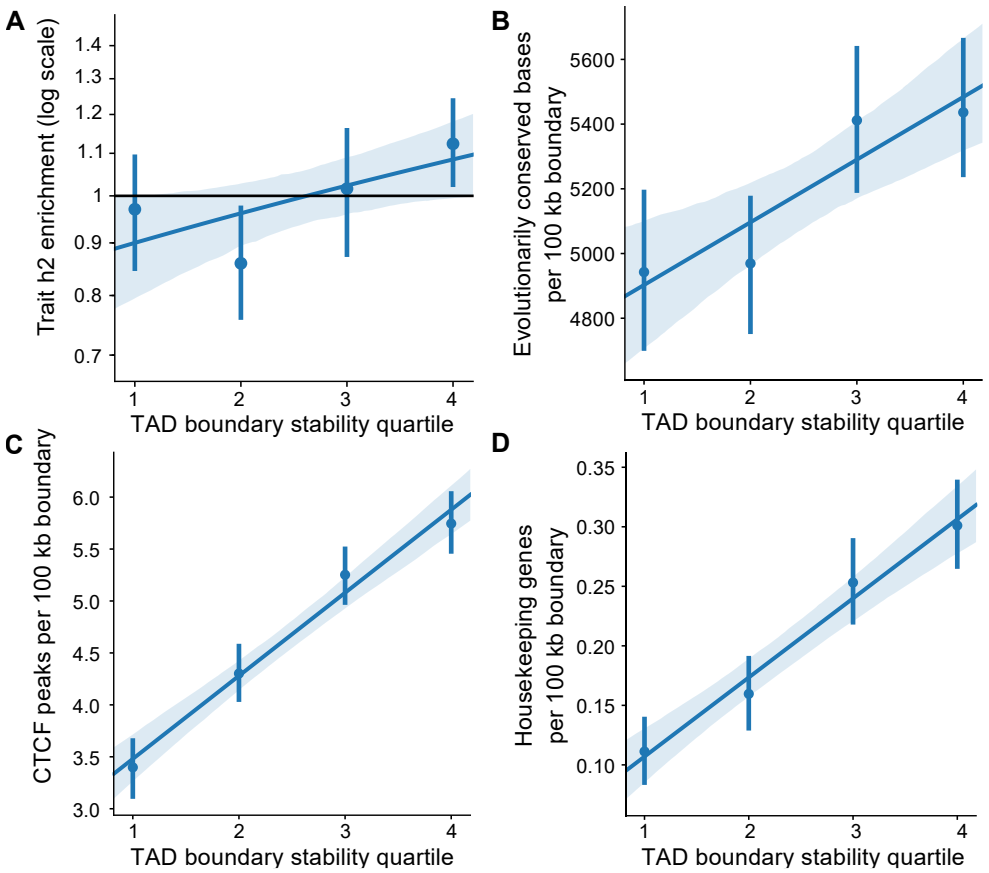

Figure S13. Removing boundaries near genomic gaps or blacklist regions increases the correlations between stability and functional attributes. In Figs. 3C-F we note that there is a positive trend between TAD boundary stability quartile and functional annotation; however, we find that the fourth quartile "drops-off" and has equal or slightly lower enrichment compared to the third quartile. We hypothesize that this trend is, in part, due to technical factors. For example, TADs must be called at the starts and ends of chromosomes, centromeres, and assembly gaps in all tissues. This may create highly stable TAD boundaries independent of their functional significance. To test this, we apply a conservative filter and remove all boundaries within 5 MB of a genomic gap or blacklist region. Across TAD boundary stability quartiles, we replicate the correlation between increased cell type stability and increased **(A)** complex trait heritability enrichment ($P = 0.03$), **(B)** conserved bases (overlap with PhastCons elements, $P = 0.0002$), **(C)** CTCF binding (overlap with ChIP-seq peaks, $P = 1x10^{-37}$), and **(D)** housekeeping genes ($P = 1x10^{-18}$). The enrichment "drop-off" is reduced or absent in the relationship with heritability, CTCF, and genes suggesting that technical bias partially contributes to a drop-off of enrichment in the fourth quartile. All error bars/bands signify 95% confidence intervals.

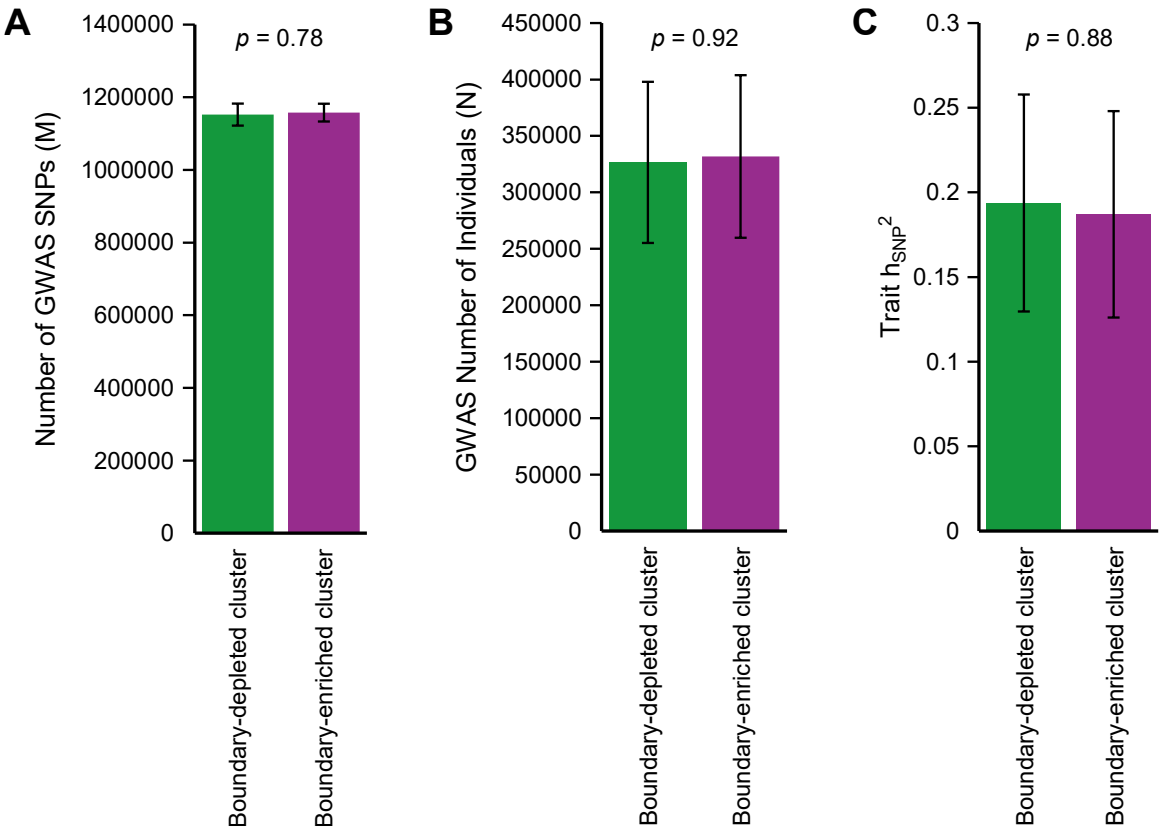

Figure S14. Traits in the boundary-depleted cluster and boundary-enriched cluster do not differ in GWAS parameters. (A) Number of GWAS SNPs (P = 0.78, t-test with equal variances), **(B)** Number of individuals in the GWAS (P = 0.92), or **(C)** SNP-based heritability (P = 0.88). Error bars signify 95% confidence intervals.

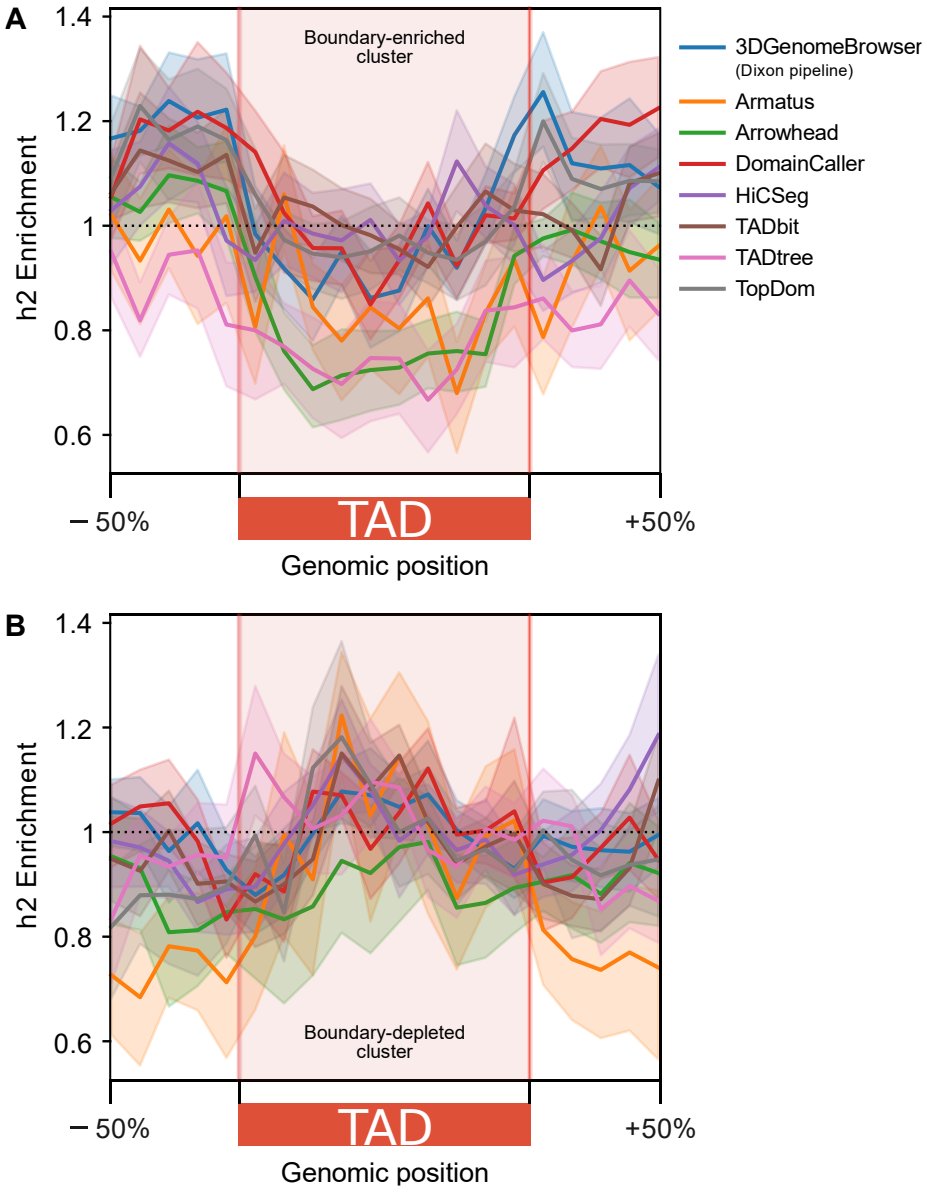

Figure S15. Patterns of heritability enrichment across the 3D genome in human embryonic stem cells (ESC) are robust to the TAD calling algorithm used. (A) Heritability enrichment landscape over TADs in ESCs called by eight different algorithms for traits in the boundary-enriched cluster. Similar to the results shown in Fig. 4B (which use TADs from the Dixon pipeline), regions flanking TADs are enriched for heritability compared to TADs. **(B)** Heritability enrichment landscape over TADs in ESCs for traits in the boundary-depleted cluster. Similar to the results shown in Fig. 4C (which use TADs from the Dixon pipeline), TADs are centrally enriched for heritability. Error bands signify 95% confidence intervals.

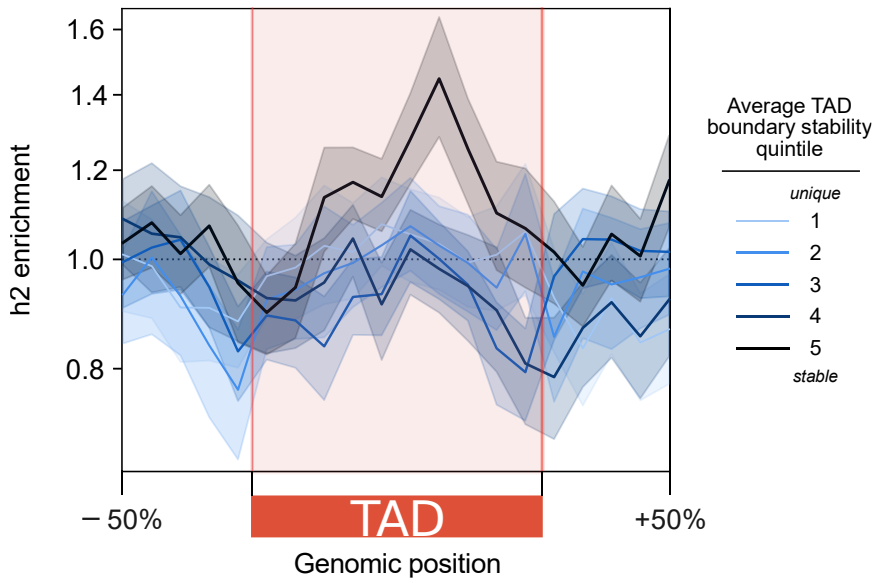

Figure S16. Among boundary-depleted traits, stable boundaries associate with stronger heritability enrichment in TAD centers. For the boundary-depleted cluster traits, TADs flanked by the most stable boundaries (measured by taking the average stability of its two boundaries and binning into quintiles) have increased heritability in the TAD center. This analysis was performed in a random subset of 7 cell types (aorta, H1_ESC, leftVentricle, Liver, psoasMuscle, SKNDZ, T470). Error bands signify 95% confidence intervals.

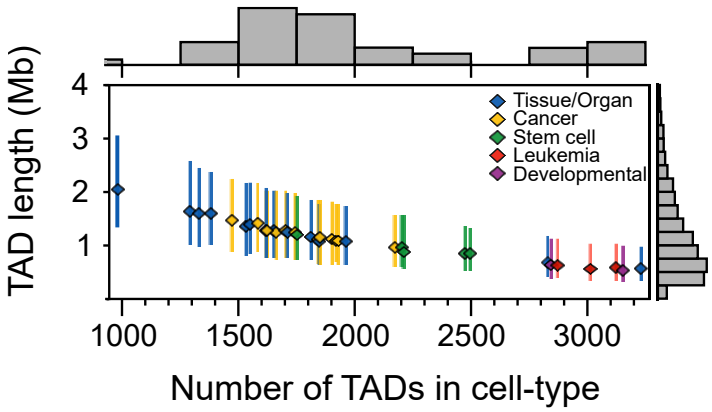

Figure S17. Average TAD length in a cell type negatively correlates with number of TADs. Across 37 cell types, there is an inverse relationship between TAD length and number of TADs. Organ/tissue cell types generally have the longest (and fewest) TADs. Leukemia and stem cells have the shortest (and most) TADs. Error bands signify the IQR.

Supplemental Table 1. Cell types used for all analyses from the 3DGenomeBrowser

FileNameFrom3DGenomeBrowser	CellTypeDescription	Abbreviation	BiologicalCluster	GermLayer	Citation
A549_raw-rep1_TADs.txt	A549_lungAdenocarcinoma_dekker	A549	cancer	endoderm	Lajoie, Dekker et al. (2015)[8], ENCODE[9,10]
AdrenalGland_Donor-AD2-raw_TADs.txt	adrenal_schmitt2016	adrenal	organ/tissue	endoderm	Schmitt et al. (2016)[7]
Aorta_STL002_Leung2015-raw_TADs.txt	aorta_leung2015	aorta	organ/tissue	mesoderm	Leung et al. (2015)[11]
Bladder_Donor-BL1-raw_TADs.txt	bladder_schmitt2016	bladder	organ/tissue	endoderm	Schmitt et al. (2016)[7]
Bowel_Small_Donor-SB2-raw_TADs.txt	smallBowel_schmitt2016	smallBowel	organ/tissue	endoderm	Schmitt et al. (2016)[7]
Caki2_raw-rep1_TADs.txt	Caki2_clearCellRenalCellCarcinoma_dekker	Caki2	cancer	mesoderm	Lajoie, Dekker et al. (2015)[8], ENCODE[9,10]
Cortex_DLPFC_Donor-CO-raw_TADs.txt	cortex_DLPFC_schmitt2016	DLPFC	organ/tissue	ectoderm	Schmitt et al. (2016)[7]
G401_raw-rep1_TADs.txt	G401_Wilms_tumor_dekker	G401	cancer	mesoderm	Lajoie, Dekker et al. (2015)[8], ENCODE[9,10]
GM12878_Lieberman-raw_TADs.txt	GM12878_lymphoblastoid_Lieberman	GM12878	leukemia	mesoderm	Rao et al. (2014)[6]
H1-ESC_Dixon2015-raw_TADs.txt	H1_ESC_Dixon2015	ESC	stem cell	NA	Dixon et al. (2015)[12]
H1-MES_Dixon2015-raw_TADs.txt	H1_mesendoderm_Dixon2015	MES	stem cell	NA	Dixon et al. (2015)[12]
H1-MSC_Dixon2015-raw_TADs.txt	H1_mesenchymalSC_Dixon2015	MSC	stem cell	mesoderm	Dixon et al. (2015)[12]
H1-NPC_Dixon2015-raw_TADs.txt	H1_neuralSC_Dixon2015	NPC	stem cell	ectoderm	Dixon et al. (2015)[12]
H1-TRO_Dixon2015-raw_TADs.txt	H1_trophoblastLike_Dixon2015	TRO	stem cell	NA	Dixon et al. (2015)[12]
HMEC_Lieberman-raw_TADs.txt	HMEC_humanMammaryEpithelial_Lieberman	HMEC	organ/tissue	ectoderm	Rao et al. (2014)[6]
HUVEC_Lieberman-raw_TADs.txt	HUVEC_Lieberman	HUVEC	organ/tissue	mesoderm	Rao et al. (2014)[6]
IMR90_Lieberman-raw_TADs.txt	IMR90_fetalLungFibroblast_Lieberman	IMR90	organ/tissue	endoderm	Rao et al. (2014)[6]
K562_Lieberman-raw_TADs.txt	K562_CML_Lieberman	K562	leukemia	mesoderm	Rao et al. (2014)[6]
KBM7_Lieberman-raw_TADs.txt	KBM7_CML_Lieberman	KBM7	leukemia	mesoderm	Rao et al. (2014)[6]
Liver_STL011_Leung_2015-raw_TADs_hg19From38.txt	Liver_leung2015	Liver	organ/tissue	endoderm	Leung et al. (2015)[11]
LNCaP_raw-rep1_TADs.txt	LNCaP_prostateAdenocarcinoma_dekker	LNCaP	cancer	endoderm	Lajoie, Dekker et al. (2015)[8], ENCODE[9,10]
Lung_Donor-LG1-raw_TADs.txt	lung_schmitt2016	lung	organ/tissue	endoderm	Schmitt et al. (2016)[7]
Muscle_Psoas_Donor-PO1-raw_TADs.txt	psoasMuscle_schmitt2016	psoas	organ/tissue	mesoderm	Schmitt et al. (2016)[7]
NCIH460_raw-rep1_TADs.txt	NCIH460_NSCLC_dekker	NCIH460	cancer	endoderm	Lajoie, Dekker et al. (2015)[8], ENCODE[9,10]
NHEK_Lieberman-raw_TADs.txt	NHEK_epidermalKeratinocytes_Lieberman	NHEK	organ/tissue	ectoderm	Rao et al. (2014)[6]
PANC1_raw-rep1_TADs.txt	PANC1_pancreaticCarcinoma_dekker	PANC1	cancer	endoderm	Lajoie, Dekker et al. (2015)[8], ENCODE[9,10]
Pancreas_Donor-PA2-raw_TADs.txt	pancreas_schmitt2016	pancreas	organ/tissue	endoderm	Schmitt et al. (2016)[7]
RPMI7951_raw-rep1_TADs.txt	RPMI7951_melanoma_dekker	RPMI7951	cancer	ectoderm	Lajoie, Dekker et al. (2015)[8], ENCODE[9,10]
SJCRH30_raw-rep1_TADs.txt	SJCRH30_BMrhabdomyosarcoma_dekker	SJCRH30	cancer	mesoderm	Lajoie, Dekker et al. (2015)[8], ENCODE[9,10]
SKMEL5_raw-rep1_TADs.txt	SKMEL5_melanoma_dekker	SKMEL5	cancer	ectoderm	Lajoie, Dekker et al. (2015)[8], ENCODE[9,10]
SKNDZ_raw-rep1_TADs.txt	SKNDZ_neurblastoma_dekker	SKNDZ	cancer	ectoderm	Lajoie, Dekker et al. (2015)[8], ENCODE[9,10]
SKNMC_raw-rep1_TADs.txt	SKNMC_neuroblastoma_dekker	SKNMC	cancer	ectoderm	Lajoie, Dekker et al. (2015)[8], ENCODE[9,10]
Spleen_Donor-PX1-raw_TADs.txt	spleen_schmitt2016	spleen	organ/tissue	mesoderm	Schmitt et al. (2016)[7]
T470_raw-rep1_TADs.txt	T470_breastCancer_dekker	T470	cancer	ectoderm	Lajoie, Dekker et al. (2015)[8], ENCODE[9,10]
Thymus_STL001_Leung2015-raw_TADs.txt	thymus_leung2015	thymus	organ/tissue	endoderm	Leung et al. (2015)[11]
VentricleLeft_STL003_Leung2015-raw_TADs.txt	leftVentricle_leung2015	leftVentricle	organ/tissue	mesoderm	Leung et al. (2015)[11]
VentricleRight_Donor-RV3-raw_TADs.txt	rightVentricle_schmitt2016	rightVentricle	organ/tissue	mesoderm	Schmitt et al. (2016)[7]

Supplemental Table 2. Genome-wide association study (GWAS) traits used for heritability analyses

Nickname	Trait	M	h2	h2_SE	N	Phenotypic class	actual cluster	Source
Anorexia	Anorexia	931184	0.2153	0.0169	32143	Neuropsych	Boundary-depleted	Boraska et al. 2014 Mol Psych[13]
ASD	Autism_Spectrum	1173307	0.4607	0.0517	10263	Neuropsych	Boundary-depleted	PGC Cross-Disorder Group, 2013 Lancet[14]
AutoimmuneDz	Auto_Immune_Traits_(Sure)	1187056	0.0068	0.0013	459324	Immunologic	Boundary-enriched	UKBiobank[15]
Balding	Balding_Type_I	1187056	0.2154	0.019	208336	Dermatologic	Boundary-depleted	UKBiobank[15]
BMI	BMI	1187056	0.252	0.0071	457824	Metabolic	Boundary-depleted	UKBiobank[15]
CrohnsDz	Crohn's_Disease	1051514	0.4723	0.0575	20883	Immunologic	Boundary-enriched	Jostins et al., 2012 Nature[16]
DepressiveSxs	Depressive_symptoms	1115393	0.0473	0.0037	161460	Neuropsych	Boundary-depleted	Okbay et al., 2016 Nat Genet[17]
DermDz	Dermatologic_Diseases	1187056	0.0094	0.0014	459324	Dermatologic	Boundary-enriched	UKBiobank[15]
Eczema	Eczema	1187056	0.0675	0.0038	458699	Dermatologic	Boundary-enriched	UKBiobank[15]
EosinophilCount	Eosinophil_Count	1187056	0.1977	0.0143	439938	Hematologic	Boundary-enriched	UKBiobank[15]
FEV1_FVC_Ratio	FEV1-FVC_Ratio	1187056	0.2336	0.0113	371949	Cardiopulmonary	Boundary-enriched	UKBiobank[15]
FirstBirthAge	Age_first_birth	1079424	0.0617	0.0033	222037	Reproductive	Boundary-depleted	Barban et al., 2016 Nat Genet[18]
FVC	Forced_Vital_Capacity_(FVC)	1187056	0.2068	0.0065	371949	Cardiopulmonary	Boundary-enriched	UKBiobank[15]
HairColor	Hair_Color	1187056	0.4523	0.1497	452720	Dermatologic	Boundary-depleted	UKBiobank[15]
HDL	HDL	1019272	0.1362	0.0166	99900	Metabolic	Boundary-enriched	Teslovich et al., 2010 Nature[19]
Heel_T_Score	Heel_T_Score	1187056	0.3628	0.0307	445921	Skeletal	Boundary-depleted	UKBiobank[15]
Height	Height	1187056	0.6034	0.027	458303	Skeletal	Boundary-enriched	UKBiobank[15]
HighCholesterol	High_Cholesterol	1187056	0.0468	0.0039	459324	Metabolic	Boundary-enriched	UKBiobank[15]
Hypothyroidism	Hypothyroidism	1187056	0.0459	0.0037	459324	Metabolic	Boundary-enriched	UKBiobank[15]
LDL	LDL	1017973	0.121	0.0166	95454	Metabolic	Boundary-enriched	Teslovich et al., 2010 Nature[19]
MenarcheAge	Age_at_Menarche	1187056	0.2457	0.0102	242278	Reproductive	Boundary-enriched	UKBiobank[15]
MenopauseAge	Age_at_Menopause	1187056	0.1215	0.0086	143025	Reproductive	Boundary-enriched	UKBiobank[15]
MorningPerson	Morning_Person	1187056	0.1002	0.0035	410520	Neuropsych	Boundary-depleted	UKBiobank[15]
Neuroticism	Neuroticism	1187056	0.1113	0.0037	372066	Neuropsych	Boundary-depleted	UKBiobank[15]
NumChildrenBorn	Number_children_ever_born	1080059	0.0256	0.0018	318863	Reproductive	Boundary-depleted	Barban et al., 2016 Nat Genet[18]
PlateletCount	Platelet_Count	1187056	0.349	0.0294	444382	Hematologic	Boundary-enriched	UKBiobank[15]
RA	Rheumatoid_Arthritis	1125155	0.1694	0.023	38242	Immunologic	Boundary-enriched	Okada et al., 2014 Nature[20]
RBCCount	Red_Blood_Cell_Count	1187056	0.2434	0.0191	445174	Hematologic	Boundary-enriched	UKBiobank[15]
RDW	Red_Blood_Cell_Distribution_Width	1187056	0.2234	0.0198	442700	Hematologic	Boundary-enriched	UKBiobank[15]
Resp_ENT_Dz	Respiratory_and_Ear-nose-throat_Diseases	1187056	0.0483	0.0034	459324	Cardiopulmonary	Boundary-depleted	UKBiobank[15]
Schizophrenia	Schizophrenia	1083014	0.4512	0.0189	70100	Neuropsych	Boundary-depleted	SCZ Working Group of the PGC, 2014 Nature[21]
SkinColor	Skin_Color	1187056	0.1896	0.0539	453609	Dermatologic	Boundary-depleted	UKBiobank[15]
SmokingStatus	Smoking_Status	1187056	0.0972	0.0032	457683	Neuropsych	Boundary-depleted	UKBiobank[15]
Sunburn	Sunburn_Occasion	1187056	0.0915	0.0162	344229	Dermatologic	Boundary-depleted	UKBiobank[15]
SystolicBP	Systolic_Blood_Pressure	1187056	0.1966	0.007	422771	Cardiopulmonary	Boundary-depleted	UKBiobank[15]
T2D	Type_2_Diabetes	1187056	0.043	0.0025	459324	Metabolic	Boundary-enriched	UKBiobank[15]
Tanning	Tanning	1187056	0.172	0.0609	449984	Dermatologic	Boundary-depleted	UKBiobank[15]
UC	Ulcerative_Colitis	1076834	0.2424	0.032	27432	Immunologic	Boundary-enriched	Jostins et al., 2012 Nature[16]
WaistHipRatio	Waist-hip_Ratio	1187056	0.1423	0.0067	458417	Metabolic	Boundary-enriched	UKBiobank[15]
WBCCount	White_Blood_Cell_Count	1187056	0.1873	0.0105	444502	Hematologic	Boundary-enriched	UKBiobank[15]
YearsOfEd	College_Education	1187056	0.1299	0.0037	454813	Neuropsych	Boundary-depleted	UKBiobank[15]

REFERENCES FOR SUPPLEMENTAL INFORMATION

1. Hinrichs, A.S., Karolchik, D., Baertsch, R., Barber, G.P., Bejerano, G., Clawson, H., Diekhans, M., Furey, T.S., Harte, R.A., Hsu, F., et al. (2006). The UCSC Genome Browser Database: update 2006. Nucleic Acids Res. *34*, D590–D598.
2. Haeussler, M., Zweig, A.S., Tyner, C., Speir, M.L., Rosenbloom, K.R., Raney, B.J., Lee, C.M., Lee, B.T., Hinrichs, A.S., Gonzalez, J.N., et al. (2019). The UCSC Genome Browser database: 2019 update. Nucleic Acids Res.
3. Bonev, B., Mendelson Cohen, N., Szabo, Q., Fritsch, L., Papadopoulos, G.L., Lubling, Y., Xu, X., Lv, X., Hugnot, J.-P., Tanay, A., et al. (2017). Multiscale 3D Genome Rewiring during Mouse Neural Development. Cell *171*, 557-572.e24.
4. Sauerwald, N., and Kingsford, C. (2018). Quantifying the similarity of topological domains across normal and cancer human cell types. Bioinformatics *34*, i475–i483.
5. Sauerwald, N., Singhal, A., and Kingsford, C. (2020). Analysis of the structural variability of topologically associated domains as revealed by Hi-C. NAR Genomics Bioinforma. *2*,.
6. Rao, S.S.P., Huntley, M.H., Durand, N.C., Stamenova, E.K., Bochkov, I.D., Robinson, J.T., Sanborn, A.L., Machol, I., Omer, A.D., Lander, E.S., et al. (2014). A 3D Map of the Human Genome at Kilobase Resolution Reveals Principles of Chromatin Looping. Cell *159*, 1665–1680.
7. Schmitt, A.D., Hu, M., Jung, I., Xu, Z., Qiu, Y., Tan, C.L., Li, Y., Lin, S., Lin, Y., Barr, C.L., et al. (2016). A Compendium of Chromatin Contact Maps Reveals Spatially Active Regions in the Human Genome. Cell Rep. *17*, 2042–2059.
8. Lajoie, B.R., Dekker, J., and Kaplan, N. (2015). The Hitchhiker's guide to Hi-C analysis: Practical guidelines. Methods *72*, 65–75.
9. ENCODE Project Consortium (2012). An integrated encyclopedia of DNA elements in the human genome. Nature *489*, 57–74.
10. Davis, C.A., Hitz, B.C., Sloan, C.A., Chan, E.T., Davidson, J.M., Gabdank, I., Hilton, J.A., Jain, K., Baymuradov, U.K., Narayanan, A.K., et al. (2018). The Encyclopedia of DNA elements (ENCODE): data portal update. Nucleic Acids Res. *46*, D794–D801.
11. Leung, D., Jung, I., Rajagopal, N., Schmitt, A., Selvaraj, S., Lee, A.Y., Yen, C.A., Lin, S., Lin, Y., Qiu, Y., et al. (2015). Integrative analysis of haplotype-resolved epigenomes across human tissues. Nature *518*, 350–354.
12. Dixon, J.R., Jung, I., Selvaraj, S., Shen, Y., Antosiewicz-Bourget, J.E., Lee, A.Y., Ye, Z., Kim, A., Rajagopal, N., Xie, W., et al. (2015). Chromatin architecture reorganization during stem cell differentiation. Nature *518*, 331–336.
13. Boraska, V., Franklin, C.S., Floyd, J.A.B., Thornton, L.M., Huckins, L.M., Southam, L., Rayner, N.W., Tachmazidou, I., Klump, K.L., Treasure, J., et al. (2014). A genome-wide association study of anorexia nervosa. Mol. Psychiatry.
14. Smoller, J.W., Kendler, K., Craddock, N., Lee, P.H., Neale, B.M., Nurnberger, J.N., Ripke, S., Santangelo, S., Sullivan, P.S., Neale, B.N., et al. (2013). Identification of risk loci with shared effects on five major psychiatric disorders: A genome-wide analysis. Lancet.
15. Sudlow, C., Gallacher, J., Allen, N., Beral, V., Burton, P., Danesh, J., Downey, P., Elliott, P., Green, J., Landray, M., et al. (2015). UK Biobank: An Open Access Resource for Identifying the Causes of a Wide Range of Complex Diseases of Middle and Old Age. PLoS Med. *12*, e1001779.
16. Jostins, L., Ripke, S., Weersma, R.K., Duerr, R.H., McGovern, D.P., Hui, K.Y., Lee, J.C., Philip Schumm, L., Sharma, Y., Anderson, C.A., et al. (2012). Host-microbe interactions have shaped the genetic architecture of inflammatory bowel disease. Nature.
17. Okbay, A., Baselmans, B.M.L., De Neve, J.E., Turley, P., Nivard, M.G., Fontana, M.A., Meddens, S.F.W., Linnér, R.K., Rietveld, C.A., Derringer, J., et al. (2016). Genetic variants associated with subjective well-being, depressive symptoms, and neuroticism identified through genome-wide analyses. Nat. Genet.
18. Barban, N., Jansen, R., De Vlaming, R., Vaez, A., Mandemakers, J.J., Tropf, F.C., Shen, X., Wilson, J.F., Chasman, D.I., Nolte, I.M., et al. (2016). Genome-wide analysis identifies 12 loci influencing human reproductive behavior. Nat. Genet.
19. Teslovich, T.M., Musunuru, K., Smith, A. V., Edmondson, A.C., Stylianou, I.M., Koseki, M., Pirruccello, J.P., Ripatti, S., Chasman, D.I., Willer, C.J., et al. (2010). Biological, clinical and population relevance of 95 loci for blood lipids. Nature.
20. Okada, Y., Wu, D., Trynka, G., Raj, T., Terao, C., Ikari, K., Kochi, Y., Ohmura, K., Suzuki, A., Yoshida, S., et al. (2014). Genetics of rheumatoid arthritis contributes to biology and drug discovery. Nature.
21. Ripke, S., Neale, B.M., Corvin, A., Walters, J.T.R., Farh, K.H., Holmans, P.A., Lee, P., Bulik-Sullivan, B., Collier, D.A., Huang, H., et al. (2014). Biological insights from 108 schizophrenia-associated genetic loci. Nature.